ACS OMEGA

http://pubs.acs.org/journal/acsodf

Article

Single Crystallization of Cs_4PbBr_6 Perovskite from Supersaturated Organic Solutions Optimized Through Solubility Studies

Satoshi Watanabe,* Taiki Hayashida, Masaru Iwai, Yusuke Inomata, Masashi Kunitake, and Tetsuya Kida*

Cite This: *ACS Omega* 2023, 8, 2455−2461

Read Online

ACCESS | Metrics & More | Article Recommendations | Supporting Information

ABSTRACT: We demonstrate the fabrication of millimeter-sized single crystals of 0D-Cs_4PbBr_6 grown in a supersaturated solution consisting of organic solvents without HBr (aq). One of the precursors, CsBr, was dissolved in ethylene glycol (EG) mixed with dimethyl sulfoxide, which is a good solvent for the other precursor, $PbBr_2$. At a solvent ratio of 20 vol % EG, the solubility of cesium bromide decreased and the title compound, Cs_4PbBr_6, was selectively formed, whereas, with an EG ratio of 80 vol %, 3D-$CsPbBr_3$ was formed. A phase diagram (solubility curve) of Cs_4PbBr_6 in the mixed solvent containing 20 vol % EG was obtained by visually observing dissolution and crystal precipitation while changing the temperature. Because the solubility was proportional to the temperature, the solubility curve demonstrated an upper critical solution phenomenon. The solubility near the boiling point of the solution (150 °C) was approximately 0.14 M. A single crystal of Cs_4PbBr_6 was formed by growing a seed crystal in a supersaturated solution on the low-temperature side of the solubility curve. X-ray analysis established the crystal structure; a fluorescence emission at 520 nm with a full width at half maximum of 20 nm confirms the composition of the single crystal to be Cs_4PbBr_6.

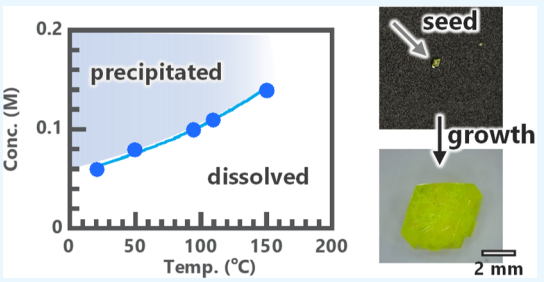

INTRODUCTION

Inorganic lead halide perovskite materials have attracted much attention because of their unique light and electronic properties such as having a high light absorption coefficient, a long lifetime of photo-excited carriers, and high quantum efficiency.[1,2,9] The band gap and Fermi level of lead halide perovskite materials can be tuned by adjusting the chemical species or changing the composition or phase.[3] A difference in the crystal structure is observed with a change in the halide composition of the perovskite. $CsPbX_3$ (X = halide) with a three-dimensional crystal lattice structure, $CsPb_2X_5$ with a two-dimensional crystal structure,[4] and Cs_4PbBr_6 with a zero-dimensional crystal structure are well known.[5] In $CsPbX_3$, the conjugated system extends in three dimensions, leading to a narrow band gap. These characteristics are suitable for solar cells and light-emitting diodes.[6] $CsPb_2X_5$ is characterized by its possession of a wide band gap in the deep ultraviolet region due to limited conjugation within the two-dimensional layer crystal lattice. In Cs_4PbBr_6, the PbX_6^{4-}octahedral unit is completely detached from the conjugation of the band structures, making the perovskite less susceptible to the external environment and internal defects of the crystals. These factors lead to high quantum efficiency and narrow bandwidth of the fluorescence in bulk crystals.

To fabricate the devices and evaluate the physical properties of these inorganic lead halide perovskite materials, the development of fabrication processes of the nanoparticles or bulk crystals is important. This fabrication process requires good control over the sizes, shapes (including crystal orientation), number of defects (including voids), and purities of the crystals.

Obtaining large, pure crystals is usually achieved via dissolution, followed by the precipitation of the desired material from solutions to fine-tune the rate of crystallization. Dimethyl sulfoxide (DMSO) and *N*,*N*-dimethylformamide are often used as good solvents, and methanol and dichloromethane are often used as poor solvents. In an early report to prepare single crystals, simple methods were used such as solvent evaporation from the solution or exposure of the solution to a poor solvent.[7,8] After that study, solubility curves of systematic solubility studies of the inorganic lead halide perovskites in solution were reported, and several unique dissolution phenomena were observed.[9] One such phenomenon is that the solubilities of the inorganic lead halide perovskites were constant regardless of the temperature, probably due to the low solubility of the cesium precursors.

Received: October 28, 2022
Accepted: December 21, 2022
Published: January 6, 2023

https://doi.org/10.1021/acsomega.2c06945
ACS Omega 2023, 8, 2455−2461

In the $CsPbX_3$ system, an interesting phenomenon called the lower critical solution phenomenon, wherein the solubility decreases with increasing temperature due to de-solvation over a phase-transition temperature region, was also observed and utilized for single crystallization.[10] Recently, an aqueous solution of HBr (HBr(aq)) has been reported to be a good solvent for the cesium precursor.[11] In mixed solvents of DMSO and HBr(aq), a typical upper critical solution phenomenon is observed in the solubility curve of Cs_4PbBr_6, in which solubility is proportional to temperature. This phenomenon enabled the easy preparation of supersaturated solutions, leading to the fabrication of centimeter-sized single crystals. In addition, the composition of inorganic perovskite materials could be freely controlled to yield Cs_4PbBr_6, $CsPb_2Br_5$, or $CsPbBr_3$ by changing the ratio of HBr (aq)/DMSO.[12] However, because the solubility of Cs_4PbBr_6 was at the level of several tens of mM, the solubility must be increased to fabricate larger crystals rapidly. Furthermore, volatile strong acids are difficult to apply to printing and withdrawal techniques due to the corrosion of the printing equipment and changes in pH due to volatilization. In this study, we prepared the solubility curves of Cs_4PbBr_6 in a mixture of ethylene glycol (EG) (a good solvent for the precursor CsBr) and DMSO, and we fabricated single crystals by cooling a supersaturated solution with the optimal solvent ratio found in the solubility studies.

EXPERIMENT

Materials. Cesium bromide (purity: 99.9%), dimethyl sulfoxide (DMSO), methanol, 48 wt % hydrobromic acid, EG, 1,2-dichloroethane, and *N*, *N*-dimethylformamide were purchased from FUJIFILM Wako Pure Chemical Corporation (Japan). Lead bromide (purity: 99.9%) was obtained from Tokyo Chemical Industry Co., Ltd (Japan). These chemicals were used in the air without any further purification.

Solubility Curve Experiments. Samples for the experiments about the results in Figures 1 and 4 were prepared by the following procedure. A predetermined amount of cesium bromide, lead bromide, or the mixture [CsBr: $PbBr_2$ = 4:1 (mol)] was added to 1 mL of the appropriate pure or mixed solvent in a 1 mL sample tube with a diameter of approximately 0.7 cm. The sample tubes were set in the holes of an aluminum block on an RCH-1000 hot plate (Tokyo Rikakikai Co, Ltd). A feedback sensor was set in a sample tube. The temperature was raised by 1 °C every 1 h. While maintaining the temperature, the samples were mixed with a vortex mixer once every 10 min. The temperature at which the powder was seen by the eye to be completely dissolved was defined as the dissolution temperature at that concentration, which defines the solubility of the substance at that temperature. After complete dissolution, an additional known amount of the powder was added to the sample tubes until some powder remained undissolved, to find out the dissolution temperature of the higher concentration. This procedure was repeated until the temperature was close to the boiling point of the solvent.

In the experiment related to the results in Figure 2a–c, the dissolution concentration was observed only at 25, 60, and 100 °C, respectively. The temperature was kept constant and the precursor powders were added little by little to a mixture of EG and DMSO at EG ratios of 0, 25, 50, 85, and 100 vol %. Near the dissolution concentration, the powders were added with an accuracy of 1.0–10.0 mg in weight.

In the experiment for which the results are plotted in Figure 3, precipitated crystals in the saturated solution were visually observed to investigate the stable crystal phase. The initial concentrations of CsBr and $PbBr_2$ were 0.60 and 0.15 M, respectively (Cs/Pb = 4/1 (mol/mol)), and the solvents were a mixture of EG and DMSO at a ratio of 20 and 80 vol % EG, respectively. The temperature was raised from room temperature to 100 °C and then allowed to cool to room temperature

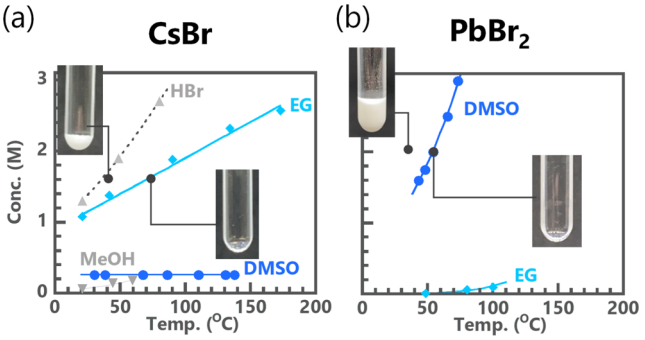

Figure 1. Solubility curves of (a) CsBr in HBr (aq), EG, MeOH, and DMSO and (b) $PbBr_2$ in EG and DMSO. The inset images are photographs of (a) CsBr in EG and (b) $PbBr_2$ in DMSO below and above the dissolution temperature at the saturation concentration.

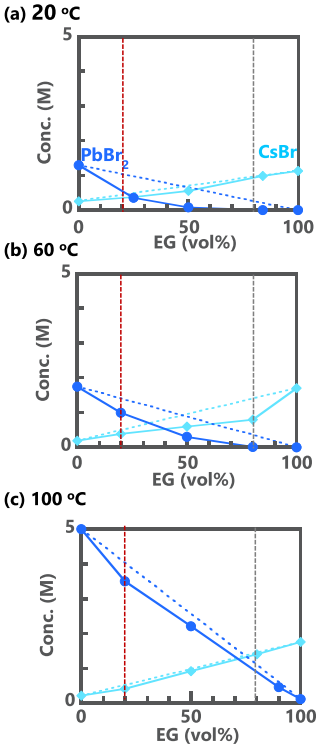

Figure 2. Concentration of CsBr or $PbBr_2$ plotted against EG ratios of 0, 25, 50, 80, and 100 vol % in the mixed-solvent system of EG and DMSO at (a) 20, (b) 60, and (c) 100 °C, respectively. The plots show the dissolution points of CsBr (light blue diamonds) and $PbBr_2$ (dark blue circles). The solid lines connect each data point for each substance, and the dotted lines represent the ideal change in solubility as the solvent ratio varies from 0 to 100 vol %. The vertical red and gray dotted lines emphasize the EG ratios of 20 and 80 vol %, respectively.

https://doi.org/10.1021/acsomega.2c06945
ACS Omega 2023, 8, 2455−2461

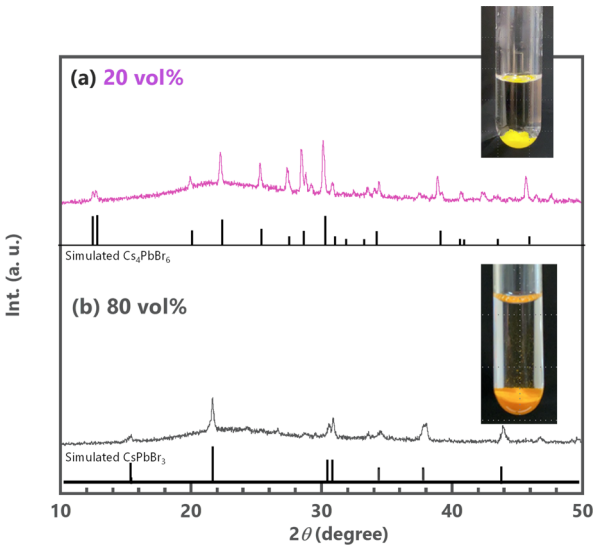

Figure 3. X-ray diffraction patterns of the powders precipitated in the solution consisting of CsBr and $PbBr_2$ and the mixed EG/DMSO solvents at EG ratios of (a) 20 and (b) 80 vol %. The concentrations of CsBr and $PbBr_2$ were 0.60 and 0.15 M, respectively [Cs/Pb = 4/1 (mol/mol)].

by natural cooling. At this point, the precipitated crystals were harvested by filtration and dried, and the powder X-ray diffraction pattern was measured.

Crystallization from a Supersaturated Solution. CsBr and $PbBr_2$ were added to 5 mL of a mixed-solvent system of EG and DMSO (20/80 v/v) to concentrations of 0.4 and 0.1 M, respectively. The samples were heated at 130 °C for 1 h to dissolve the powders completely. Each solution was passed through a 0.80 μm disposable filter (Advantech, Japan) to remove undissolved solids. First, the heated solutions were cooled down to room temperature to fabricate seed crystals. The seed crystals were taken out of the solution with tweezers. Next, the seed crystals were put gently in the supersaturated solution that was prepared by cooling a fresh solution from 130 to 100 °C ($PbBr_2$ saturated condition). The solution with seed crystals was cooled down to 20 °C (saturated concentration 0.06 M of $PbBr_2$) at a rate of 0.35 °C h^{-1}. Upon reaching 20 °C, the theoretical $PbBr_2$ supersaturation concentration was 0.04; multiplying this concentration by the volume of the solution (5 mL) would mean that 0.2 mmol of the molecules should be precipitated. If the molecular weight of Cs_4PbBr_6 was 1218 g mol^{-1} and the density was 4.00 g mL^{-1}, the volume of the formed single crystal should be 54 mm^3, assuming that the 0.2 mmol molecules crystallized. After satisfactory crystal growth was achieved, the single crystal was taken out of the solution with tweezers.

Characterization. The powder X-ray diffraction pattern was measured with a Mini Flex 600 spectrometer (Rigaku Corporation, Japan) with an X-ray source of CuKα (40 kV, 15 mA), a scan speed of 10° min^{-1}, and a scan step of 0.02°. Absorption and luminescence spectra of the crystals were obtained with diffuse reflection cells by crushing the crystals into a powder in a mortar and molding the cells with barium sulfate. Ultraviolet−visible spectra were obtained from a V-660 spectrometer (Jasco, Japan) at room temperature, with a scan speed of 1000 nm min^{-1}, a bandwidth of 2 nm, and a data step of 0.5 nm. Photoluminescence spectra were measured with a V-8300 spectrometer (JASCO, Japan) at room temperature, using an exciting wavelength of 365 nm, a scanning speed of 500 nm min^{-1}, a bandwidth of excited and luminescent light of 5 nm, and a data step of 0.5 nm. Optical and fluorescence microscopy were measured with an RX-100 digital microscope (Hirox Co., Ltd., Japan) equipped with an optical zoom lens of HR-2016 and a halogen lamp. For cross-sectional views, the image composition function of the microscope was used to obtain a three-dimensional image by synthesizing photographs with different focal depths. Ultraviolet light for the excitation of fluorescence was obtained with a 365 nm lamp.

RESULTS AND DISCUSSION

The solubility of Cs_4PbBr_7 solutions depended on the temperature in the mixed solvent system consisting of HBr (aq).[11] Good solvents are known to be hydrobromic acid for cesium bromide and DMSO or *N*, *N*-dimethylformamide for lead bromide. The solubility of cesium bromide in organic solvents with boiling points higher than that of water, such as EG, DMSO, and methanol, was investigated in the absence of volatile acids.

Figure 1a shows the saturated concentration curves of cesium bromide in the solvents HBr(aq), EG, MeOH, and DMSO. The inset photograph at 1.6 M and 40 °C shows that cesium bromide precipitated under these conditions in EG. When the temperature was raised at a heating rate of 1 °C per 60 min, the amount of powder gradually decreased until it dissolved completely at 70 °C. This temperature was plotted as the dissolution temperature by a diamond mark in Figure 1a. The experiment was performed at a sufficiently slow heating rate of 1 °C per 60 min.

Similar experiments were repeated for concentrations of CsBr from 1 to 2.5 M. The dissolution temperature increased with an increase in concentration. For the hydrobromic acid solution, the dissolution temperatures of cesium bromide at 1.2 and 2.6 M were approximately 20 and 80 °C, respectively. For the MeOH solutions, the dissolution temperatures at 0.06 and 0.18 M were about 20 and 60 °C, respectively. For the DMSO solutions, 0.26 M cesium bromide dissolved, regardless of temperature. These results indicate that the solubility of cesium bromide in EG increases proportionally with temperature and becomes comparable to the solubility in HBr (aq) (2.5 M) when heated to 170 °C.

Figure 1b shows the solubility curves of lead bromide in EG and DMSO. The inset photographs of lead bromide in DMSO show that at a concentration of 2 M at 30 °C, lead bromide powder precipitated; heating caused this precipitate to decrease and to dissolve completely at 54 °C. A similar study at concentrations from 1.6 to 3.0 M showed that the dissolution temperature increased with increasing concentration. Lead bromide was much less soluble in EG than in DMSO, dissolving only up to 0.1 M in EG even when the temperature was raised to 100 °C.

Although the solubility of cesium bromide in EG is 2.6 M at 170 °C, EG alone hardly dissolved lead bromide. A mixed-solvent system of EG and DMSO was used to dissolve both cesium bromide and lead bromide. Figure 2 shows the dissolution concentration of cesium bromide or lead bromide at (a) 20, (b) 60, and (c) 100 °C while varying the ratio of EG to DMSO. The saturated concentrations of cesium bromide and lead bromide in pure solvents (EG = 0, 100 vol %) were connected by dotted lines, as the ideal line based on the additive property. The actual saturation concentration curve shifted below the ideal lines, indicating that the solubilities of

https://doi.org/10.1021/acsomega.2c06945
ACS Omega 2023, 8, 2455−2461

CsBr and $PbBr_2$ were decreased by using the mixed-solvent system of EG and DMSO relative to their solubilities in a pure solvent. The deviation from the ideal curve (dotted line) was large for lead bromide and small for cesium bromide, probably due to the interaction between EG and DMSO weakening the interaction between the solvent and lead bromide.

By changing the ratio of EG to DMSO, the solubilities of cesium bromide and lead bromide can be tuned. To form Cs_4PbBr_6 (Cs/Pb = 4) preferentially over $CsPbBr_3$ (Cs/Pb = 1) in the mixed solvent, the solubility of cesium bromide should be lower than that of lead bromide, which requires a low EG ratio in the EG/DMSO mixed solvent. To confirm this premise, the composition of the precipitates formed in the solvent systems with EG ratios of 20 and 80 vol % was established by powder X-ray diffraction and fluorescence emission spectroscopy. The concentrations of cesium bromide and lead bromide were set to 0.6 and 0.15 M (Cs/Pb = 4/1), respectively, which were higher than those of the saturated concentrations to ensure some precipitation. The point of complete dissolution was observed by eye after heating these samples to 100 °C and then cooling the solutions slowly to room temperature. The cooled samples were filtered, and the obtained powder was analyzed by powder X-ray diffraction.

Figure 3 shows the X-ray diffraction pattern and photographs of the powders obtained from the filtration after the heat treatment. At the EG ratio of 20 vol % (Figure 3a), the white powders of cesium bromide and lead bromide turned yellow when the mixed solvent was added at room temperature. Heating the solution dissolved some of the powder and did not change its color. When the solution was allowed to cool, an additional yellow precipitate formed. Looking at the X-ray diffraction pattern of this precipitate, the characteristic diffraction patterns of Cs_4PbBr_6 can be seen at 2θ of 12.5, 20.1, 22.3, 25.4, 27.3, 28.5, 30.1, 34.6, 39.0, and 45.8°.[11] Since the tiny peaks were seen such as 29.2, 37.5, 42.3, 46.5, and 47.6°, other compounds are slightly mixed. The green fluorescence emission spectrum obtained upon excitation with 360 nm light exposure also supported the formation of Cs_4PbBr_6.[13,14]

For the solution with an EG ratio of 80 vol % (Figure 3b), a mixture of white and orange powers was formed by adding the precursor powders to the solvent system at room temperature. As the solution was heated to 80 °C, the powder gradually dissolved, and the color of the precipitate became completely orange. After the samples were cooled slowly to room temperature, the precipitate remained orange in color. The X-ray diffraction pattern of the powder after filtration and drying showed the characteristic pattern of $CsPbBr_3$ at 2θ of 15.3, 21.7, 30.7, 33.8, 34.6, 38.0, 44.1, and 46.9°.[9] Since the small peaks were seen, other compounds including Cs_4PbBr_6 are slightly mixed. No fluorescence of the orange powder was observed under ultraviolet light. Thus, Cs_4PbBr_6 was formed mainly when EG = 20 vol %, and $CsPbBr_3$ formed mainly when EG = 80 vol %, probably because of low and high cesium bromide solubility, respectively.

By adjusting the EG ratio, the zero-dimensional and three-dimensional perovskites can be fabricated selectively. Next, the saturated concentration curve at 20 vol % EG was investigated, as summarized in Figure 4, to obtain Cs_4PbBr_6.

At 0.11 M of $PbBr_2$ (0.44 M of CsB_2), a yellow powder was precipitated in each solution at room temperature, as shown in the inset image of Figure 4. As the samples were gradually heated, the powders were dissolved completely at 109 °C. As the temperature returned to room temperature, the yellow

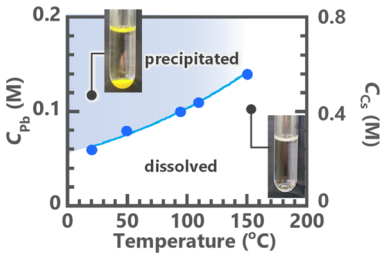

Figure 4. Solubility curve of CsBr and $PbBr_2$ in the mixed EG/DMSO solvent system at an EG ratio of 20 vol %. The y-axis (left and right) shows the concentration of $PbBr_2$ (C_{Pb}), and CsBr (C_{Cs}), respectively. CsBr was added in an amount four times that of the lead element. Inset images are photographs of the sample in precipitated and dissolved regions.

powders were reprecipitated. The dissolution temperature at $PbBr_2$ concentrations of 0.06, 0.08, 0.10, and 0.14 M was 20, 49, 94, and 150 °C, respectively. This tendency for the solubility to increase with increasing temperature is a dissolution behavior classified as an upper-critical solution phenomenon.

The red dotted line in Figure 2c shows the solubilities of CsBr and $PbBr_2$ with an EG ratio of 20 vol % at 100 °C when the initial concentrations of CsBr and $PbBr_2$ are 0.40 and 3.5 M, respectively. Compared with Figure 4, the solubility of Cs_4PbBr_6 would be determined by the solubility of cesium bromide to the mixed solvents. When the solution with 20% EG was heated close to the boiling point of EG, a higher solubility (140 mM at 150 °C) was obtained than that in the aqueous system (60 mM at 80 °C).[11]

The advantage of obtaining saturated dissolution curves is that the desired supersaturation conditions can be prepared easily. The lower the temperature (or the higher the concentration), the greater the degree of supersaturation and the faster the crystal growth rate, but the greater the risk of unintended nucleation from the bulk or from the crystal surface. For this reason, one of the general strategies for crystal growth is to grow crystals gradually with a low degree of supersaturation while maintaining a constant supersaturated concentration by lowering the temperature to compensate for the drop in concentration as the crystal grows.

In this study, a single crystal of Cs_4PbBr_6, which had been generated in a supersaturated solution, was collected, and then immersed in the saturated solution as a seed crystal for single-crystal growth.

A precipitate of fine powder was observed upon cooling the supersaturated solution used to prepare the seed crystals, and some of the crystals with characteristic shapes were observed. A submillimeter-sized quadrangular prismatic crystal (Figure 5a,c) was selected for further crystal growth by immersion into the solution (CsBr = 0.4 M and $PbBr_2$ = 0.1 M in) at 100 °C; the solution was then cooled to room temperature at a cooling rate of 0.35 °C h^{-1}. Optical microscopy images of the crystal grown in the supersaturated solution are shown in Figure 5b,d. The side of the parallelogram in the microscope image was 4 mm, and the profile showed a thickness of 2 mm. Single-crystal X-ray analysis of a typical small fragment obtained by crushing this single crystal showed a good agreement with the reported Cs_4PbBr_6 single crystals[15] (Figure S1 and Table S1). Cross-Nicol microscopy of another fabricated crystal also supports the formation of single crystals (Figure S2).

https://doi.org/10.1021/acsomega.2c06945
ACS Omega 2023, 8, 2455−2461

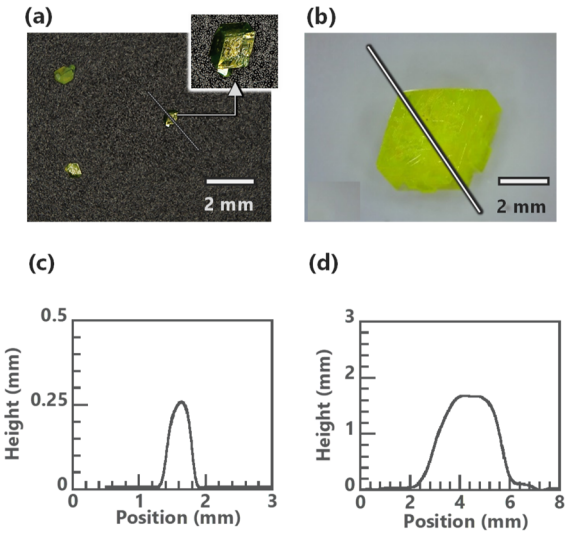

Figure 5. (a,b) Optical microscopic images and (c,d) plots of the height of a cross-section of (a,c) seed crystal and (b,d) grown crystal of Cs_4PbBr_6 on a sample stage. The grown crystal was prepared by putting a seed crystal into 5 mL of the supersaturated solution (CsBr 0.4 M, $PbBr_2$ 0.1 M) and then cooling the sample from 100 °C to room temperature at a cooling rate of 0.35 °C h^{-1}. The inset in (a) is the magnified image of the seed crystal that is profiled in (c). This seed crystal was used for single crystallization.

During crystal growth, a small amount of crystal precipitate due to unintended nucleation was present at the bottom of the sample bottle, in addition to a seed crystal. The volume of the grown crystal was about 22 mm^3, as calculated from the sizes estimated by the optical microscope. This volume corresponded to approximately 45% of the supersaturated molecules in the solution at room temperature (25 °C).

Figure 6 shows the ultraviolet−visible absorption spectrum (gray solid line), the fluorescence spectrum (green solid line),

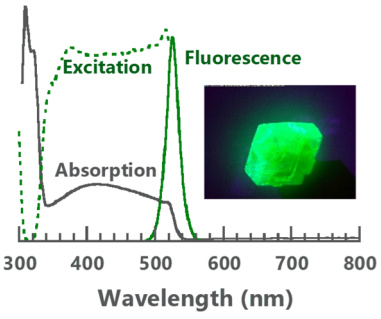

Figure 6. Ultraviolet−visible absorption (gray solid line), fluorescence (green solid line), excitation spectra (green dot line), and fluorescent microscope image of Cs_4PbBr_6 powders ground from the single crystal grown in the supersaturated solution. All vertical axes of these spectra are expressed in arbitrary units. The fluorescence spectrum and the microscope image were obtained under ultraviolet light excitation at 350 nm. The excitation spectrum was measured by scanning wavelengths below 520 nm and detecting fluorescence at 520 nm.

the excitation spectrum (green dot line), and the fluorescence microscope image (illustration) of the Cs_4PbBr_6 single crystal. The absorption spectrum was obtained by powdering the single crystal and using a diffuse reflection cell.

The ultraviolet−visible absorption spectrum showed sharp absorption bands at 306 and 326 nm, and a wide absorption band from 340 to 520 nm appeared. The sharp and wide absorption bands were attributed to the local $[PbBr_6]^{4-}$ octahedron units,[5] and $CsPbBr_3$ quantum dots,[16] respectively. Zhong et al. reported that the quantum dots partially formed in the Cs_4PbBr_6 crystals emit fluorescence.[11] Under excitation at 350 nm for fluorescence spectroscopy, fluorescence was observed at 520 nm with a full width at half maximum of 21 nm. Some reported full widths at half maximum were 16−18 nm for bulk crystals prepared by slow crystal growth[11] and 19−21 nm for quantum dots.[17,18] These indicate that more precise control of crystal growth would result in a smaller distribution of quantum dots in our crystals, leading to a narrower bandwidth of fluorescence. Fluorescent microscopy showed that the fluorescence at 520 nm can be observed over the entire crystal. The excitation spectrum shows fluorescence only with excitation light of 320−520 nm, which would support the fluorescence emission mechanism reported in previous literature.[11]

CONCLUSIONS

We demonstrate the construction of solubility diagrams and the formation of single crystals of Cs_4PbBr_6 in the EG/DMSO mixed-solvent system by increasing the solubility of cesium bromide using EG. The Cs_4PbBr_6 exhibited a typical dissolution behavior due to the upper critical solution phenomenon, in which the solubility increases with increasing temperature in EG/DMSO mixed solvent. Crystal growth was achieved by immersing prefabricated crystal seeds in supersaturated solutions and cooling gradually. These crystals emitted sharp fluorescence at 520 nm under excitation at 360 nm, which was attributed to Cs_4PbBr_6 crystals.

Intentional crystal growth in supersaturated conditions based on optimization of the solvent system through quantifying solubilities under various controlled conditions may enable intentional control of the crystal size, shape (crystal orientation), amount of introduced defects, and purity.[19,20] Altering the solvent ratio in mixed-solvent systems causes the selective formation of cesium lead halide perovskite crystals with different crystal structures.[12] As a further advantage of the EG/DMSO system, the boiling point of EG is as high as that of DMSO, which allows for high-temperature crystal growth which increases crystal growth rate and concentration. This is advantageous for the rapid fabrication of single crystals on larger or smaller scales. In addition, because highly volatile acids and water are not required, the concentration of the system is easy to keep constant. Based on these results, our research will contribute to improving the quality and shortening the fabrication time of cesium lead halide single crystals that can be applied to display backlights, scintillators, and laser emitters.

ASSOCIATED CONTENT

Supporting Information

The Supporting Information is available free of charge at https://pubs.acs.org/doi/10.1021/acsomega.2c06945.

Crystallographic structure of Cs_4PbBr_6 (CIF)

Photograph and a crystal schematic image of Cs_4PbBr_6, single-crystal X-ray analysis of a single crystal of Cs_4PbBr_6 , and optical and crossed-Nicol microscope image of a single Cs_4PbBr_6 (PDF)

https://doi.org/10.1021/acsomega.2c06945
ACS Omega 2023, 8, 2455−2461

AUTHOR INFORMATION

Corresponding Authors

Satoshi Watanabe − *Faculty of Advanced Science and Technology, Kumamoto University, Kumamoto City, Kumamoto 860-8555, Japan;* orcid.org/0000-0003-1291-1509; Email: kunitake@kumamoto-u.ac.jp

Tetsuya Kida − *Institute of Industrial Nanomaterials, Kumamoto University, Kumamoto City, Kumamoto 860-8555, Japan;* orcid.org/0000-0001-9357-9557; Email: tetsuya@kumamoto-u.ac.jp

Authors

Taiki Hayashida − *Faculty of Advanced Science and Technology, Kumamoto University, Kumamoto City, Kumamoto 860-8555, Japan*

Masaru Iwai − *Faculty of Advanced Science and Technology, Kumamoto University, Kumamoto City, Kumamoto 860-8555, Japan*

Yusuke Inomata − *Faculty of Advanced Science and Technology, Kumamoto University, Kumamoto City, Kumamoto 860-8555, Japan;* orcid.org/0000-0002-1517-966X

Masashi Kunitake − *Institute of Industrial Nanomaterials, Kumamoto University, Kumamoto City, Kumamoto 860-8555, Japan;* orcid.org/0000-0001-8070-6238

Complete contact information is available at: https://pubs.acs.org/10.1021/acsomega.2c06945

Author Contributions

All authors contributed to writing this manuscript. All authors have approved the final version of the manuscript.

Funding

This research was supported by the Ministry of Education, Culture, Sports, Science, and Technology (grant nos. 21H01239, 20H02570, and 22H01814), the New Energy and Industrial Technology Development Organization (NEDO) (grant nos. JPNP18016 and JPNP20004), and the Toshiaki Ogasawara Memorial Foundation in Japan.

Notes

The authors declare no competing financial interest.

ACKNOWLEDGMENTS

We would like to thank Prof. Shinya Hayami at Kumamoto University for the single crystal X-ray measurements.

ABBREVIATIONS

EG	ethylene glycol
DMSO	dimethyl sulfoxide

REFERENCES

(1) Zeng, Z.; Huang, B.; Wang, X.; Lu, L.; Lu, Q.; Sun, M.; Wu, T.; Ma, T.; Xu, J.; Xu, Y.; Wang, S.; Du, Y.; Yan, C. H. Multimodal Luminescent Yb 3+ /Er 3+ /Bi 3+ -Doped Perovskite Single Crystals for X-ray Detection and Anti-Counterfeiting. *Adv. Mater.* **2020**, *32*, 2004506.

(2) Rainò, G.; Becker, M. A.; Bodnarchuk, M. I.; Mahrt, R. F.; Kovalenko, M. v.; Stöferle, T. Superfluorescence from Lead Halide Perovskite Quantum Dot Superlattices. *Nature* **2018**, *563*, 671−675.

(3) Nedelcu, G.; Protesescu, L.; Yakunin, S.; Bodnarchuk, M. I.; Grotevent, M. J.; Kovalenko, M. v. Fast Anion-Exchange in Highly Luminescent Nanocrystals of Cesium Lead Halide Perovskites (CsPbX3, X = Cl, Br, I). *Nano Lett.* **2015**, *15*, 5635−5640.

(4) De Bastiani, M.; Dursun, I.; Zhang, Y.; Alshankiti, B. A.; Yin, X.-H.; Yengel, J.; Alarousu, E.; Turedi, E.; Almutlaq, B. J.; Saidaminov, M. I.; Gereige, I.; Mitra, S.; Han, I.; Roqan, I. S.; Bredas, J.-L.; Mohammed, O. F.; Bakr, O. M. Inside Perovskites: Quantum Luminescence from Bulk Cs4PbBr6 Single Crystals. *Chem. Mater.* **2017**, *29*, 7108−7113.

(5) Cao, M.; Damji, Y.; Zhang, C.; Wu, L.; Zhong, Q.; Li, P.; Yang, D.; Xu, Y.; Zhang, Q. Low-Dimensional-Networked Cesium Lead Halide Perovskites: Properties, Fabrication, and Applications. *Small Methods* **2020**, *4*, 2000303 John Wiley and Sons Inc December 1.

(6) Hoffman, J. B.; Zaiats, G.; Wappes, I.; Kamat, P. v. CsPbBr3 Solar Cells: Controlled Film Growth through Layer-by-Layer Quantum Dot Deposition. *Chem. Mater.* **2017**, *29*, 9767−9774.

(7) Zhang, H.; Liu, X.; Dong, J.; Yu, H.; Zhou, C.; Zhang, B.; Xu, Y.; Jie, W. Centimeter-Sized Inorganic Lead Halide Perovskite CsPbBr3 Crystals Grown by an Improved Solution Method. *Cryst. Growth Des.* **2017**, *17*, 6426−6431.

(8) Chang, X.; Fang, J.; Fan, Y.; Luo, T.; Su, H.; Zhang, Y.; Lu, J.; Tsetseris, L.; Anthopoulos, T. D.; Liu, S.; Zhao, K. Printable CsPbI3 Perovskite Solar Cells with PCE of 19% via an Additive Strategy. *Adv. Mater.* **2020**, *32*, 2001243.

(9) Dirin, D. N.; Cherniukh, I.; Yakunin, S.; Shynkarenko, Y.; Kovalenko, M. v. Solution-Grown CsPbBr3 Perovskite Single Crystals for Photon Detection. *Chem. Mater.* **2016**, *28*, 8470−8474.

(10) Saidaminov, M. I.; Abdelhady, A. L.; Murali, B.; Alarousu, E.; Burlakov, V. M.; Peng, W.; Dursun, I.; Wang, L.; He, Y.; Maculan, G.; Goriely, A.; Wu, T.; Mohammed, O. F.; Bakr, O. M. High-Quality Bulk Hybrid Perovskite Single Crystals within Minutes by Inverse Temperature Crystallization. *Nat. Commun.* **2015**, *6*, 7586.

(11) Chen, X.; Zhang, F.; Ge, Y.; Shi, L.; Huang, S.; Tang, J.; Lv, Z.; Zhang, L.; Zou, B.; Zhong, H. Centimeter-Sized Cs4 PbBr6 Crystals with Embedded CsPbBr3 Nanocrystals Showing Superior Photoluminescence: Nonstoichiometry Induced Transformation and Light-Emitting Applications. *Adv. Funct. Mater.* **2018**, *28*, 1706567.

(12) Lin, Q.; Bernardi, S.; Shabbir, B.; Ou, Q.; Wang, M.; Yin, W.; Liu, S.; Chesman, A. S. R.; Fürer, S. O.; Si, G.; Medhekar, N.; Jasieniak, J.; Widmer-Cooper, A.; Mao, W.; Bach, U. Phase-Control of Single-Crystalline Inorganic Halide Perovskites via Molecular Coordination Engineering. *Adv. Funct. Mater.* **2022**, *32*, 2109442.

(13) De Bastiani, M.; Dursun, I.; Zhang, Y.; Alshankiti, B. A.; Miao, X. H.; Yin, J.; Yengel, E.; Alarousu, E.; Turedi, B.; Almutlaq, J. M.; Saidaminov, M. I.; Mitra, S.; Gereige, I.; AlSaggaf, A.; Zhu, Y.; Han, Y.; Roqan, I. S.; Bredas, J. L.; Mohammed, O. F.; Bakr, O. M. Inside Perovskites: Quantum Luminescence from Bulk Cs4PbBr6 Single Crystals. *Chem. Mater.* **2017**, *29*, 7108−7113.

(14) Quan, L. N.; Quintero-Bermudez, R.; Voznyy, O.; Walters, G.; Jain, A.; Fan, J. Z.; Zheng, X.; Yang, Z.; Sargent, E. H. Highly Emissive Green Perovskite Nanocrystals in a Solid State Crystalline Matrix. *Adv. Mater.* **2017**, *29*, 1605945.

(15) Li, Y.; Shao, W.; Chen, L.; Wang, J.; Nie, J.; Zhang, H.; Zhang, S.; Gao, R.; Ouyang, X.; Ouyang, X.; Xu, Q. Lead-halide Cs4PbBr6 single crystals for high-sensitivity radiation detection. *NPG Asia Mater.* **2021**, *13*, 13.

(16) Seth, S.; Mondal, N.; Patra, S.; Samanta, A. Fluorescence Blinking and Photoactivation of All-Inorganic Perovskite Nanocrystals CsPbBr3 and CsPbBr2I. *J. Phys. Chem. Lett.* **2016**, *7*, 266−271.

(17) Hu, G.; Qin, W.; Liu, M.; Ren, X.; Wu, X.; Yang, L.; Yin, S. Scalable Room-Temperature Synthesis of Plum-Pudding-like Cs4PbBr6/CsPbBr3 Microcrystals Exhibiting Excellent Photoluminescence. *J. Mater. Chem. C* **2019**, *7*, 4733−4739.

(18) Xu, L.; Li, J.; Fang, T.; Zhao, Y.; Yuan, S.; Dong, Y.; Song, J. Synthesis of stable and phase-adjustable CsPbBr3@Cs4PbBr6 nanocrystals via novel anion-cation reactions. *Nanoscale Adv.* **2019**, *1*, 980−988.

(19) Watanabe, S.; Urata, R.; Sato, T.; Ida, S.; Kunitake, M. Single Crystallization of an Organic Semiconductor in Hydrogel Capillaries for Transferring onto Substrates. *Cryst. Growth Des.* **2019**, *19*, 3410−3416.

(20) Watanabe, S.; Ohta, T.; Urata, R.; Sato, T.; Takaishi, K.; Uchiyama, M.; Aoyama, T.; Kunitake, M. Quasi-Phase Diagrams at Air/Oil Interfaces and Bulk Oil Phases for Crystallization of Small-Molecular Semiconductors by Adjusting Gibbs Adsorption. *Langmuir* **2017**, *33*, 8906−8913.

https://doi.org/10.1021/acsomega.2c06945
ACS Omega 2023, 8, 2455−2461